Check for updates

Arch-like microsorters with multi-modal and clogging-improved filtering functions by using femtosecond laser multifocal parallel microfabrication

BING XU,[1] WENJIN HU,[1] WENQIANG DU,[1] YANLEI HU,[1,3] CHENCHU ZHANG,[1] ZHAOXIN LAO,[1] JINCHENG NI,[1] JIAWEN LI,[1] DONG WU,[1,4] JIARU CHU,[1] AND KOJI SUGIOKA[2]

[1]*CAS Key Laboratory of Mechanical Behavior and Design of Materials, Department of Precision Machinery and Precision Instrumentation, University of Science and Technology of China, Hefei 230026, China*
[2]*Laser Technology Laboratory, RIKEN, 2-1 Hirosawa, Wako, Saitama 351-0198, Japan*
[3]*huyl@ustc.edu.cn*
[4]*dongwu@ustc.edu.cn*

Abstract: Conventional micropore membranes based size sorting have been widely applied for single-cell analysis. However, only a single filtering size can be achieved and the clogging issue cannot be completely avoided. Here, we propose a novel arch-like microsorter capable of multimodal (high-, band- and low-capture mode) sorting of particles. The target particles can pass through the front filter and are then trapped by the back filter, while the non-target particles can bypass or pass through the microsorter. This 3D arch-like microstructures are fabricated inside a microchannel by femtosecond laser parallel multifocal scanning. The designed architecture allows for particles isolation free of clogging over 20 minutes. Finally, as a proof of concept demonstration, SUM159 breast cancer cells are successfully separated from whole blood.

References and links

1. T. Thorsen, S. J. Maerkl, and S. R. Quake, "Microfluidic large-scale integration," Science **298**(5593), 580–584 (2002).
2. G. M. Whitesides, "The origins and the future of microfluidics," Nature **442**(7101), 368–373 (2006).
3. E. K. Sackmann, A. L. Fulton, and D. J. Beebe, "The present and future role of microfluidics in biomedical research," Nature **507**(7491), 181–189 (2014).
4. J. El-Ali, P. K. Sorger, and K. F. Jensen, "Cells on chips," Nature **442**(7101), 403–411 (2006).
5. P. Yager, T. Edwards, E. Fu, K. Helton, K. Nelson, M. R. Tam, and B. H. Weigl, "Microfluidic diagnostic technologies for global public health," Nature **442**(7101), 412–418 (2006).
6. D. J. Beebe, J. S. Moore, J. M. Bauer, Q. Yu, R. H. Liu, C. Devadoss, and B. H. Jo, "Functional hydrogel structures for autonomous flow control inside microfluidic channels," Nature **404**(6778), 588–590 (2000).
7. A. J. deMello, "Control and detection of chemical reactions in microfluidic systems," Nature **442**(7101), 394–402 (2006).
8. M. P. MacDonald, G. C. Spalding, and K. Dholakia, "Microfluidic sorting in an optical lattice," Nature **426**(6965), 421–424 (2003).
9. S. Nagrath, L. V. Sequist, S. Maheswaran, D. W. Bell, D. Irimia, L. Ulkus, M. R. Smith, E. L. Kwak, S. Digumarthy, A. Muzikansky, P. Ryan, U. J. Balis, R. G. Tompkins, D. A. Haber, and M. Toner, "Isolation of rare circulating tumour cells in cancer patients by microchip technology," Nature **450**(7173), 1235–1239 (2007).
10. C. W. Shields, C. D. Reyes, and G. P. López, "Microfluidic cell sorting: a review of the advances in the separation of cells from debulking to rare cell isolation," Lab Chip **15**(5), 1230–1249 (2015).
11. I. Doh, H. Yoo, Y. Cho, J. Lee, H. K. Kim, and J. Kim, "Viable capture and release of cancer cells in human whole blood," Appl. Phys. Lett. **101**(4), 043701 (2012).
12. S. Song, M. S. Kim, J. Lee, and S. Choi, "A continuous-flow microfluidic syringe filter for size-based cell sorting," Lab Chip **15**(5), 1250–1254 (2015).

13. J. P. Beech, S. H. Holm, K. Adolfsson, and J. O. Tegenfeldt, "Sorting cells by size, shape and deformability," Lab Chip **12**(6), 1048–1051 (2012).
14. S. Choi, J. M. Karp, and R. Karnik, "Cell sorting by deterministic cell rolling," Lab Chip **12**(8), 1427–1430 (2012).
15. M. Werner, F. Merenda, J. Piguet, R. P. Salathé, and H. Vogel, "Microfluidic array cytometer based on refractive optical tweezers for parallel trapping, imaging and sorting of individual cells," Lab Chip **11**(14), 2432–2439 (2011).
16. F. Bragheri, P. Minzioni, R. Martinez Vazquez, N. Bellini, P. Paiè, C. Mondello, R. Ramponi, I. Cristiani, and R. Osellame, "Optofluidic integrated cell sorter fabricated by femtosecond lasers," Lab Chip **12**(19), 3779–3784 (2012).
17. J. Nam, H. Lim, D. Kim, and S. Shin, "Separation of platelets from whole blood using standing surface acoustic waves in a microchannel," Lab Chip **11**(19), 3361–3364 (2011).
18. T. Franke, S. Braunmüller, L. Schmid, A. Wixforth, and D. A. Weitz, "Surface acoustic wave actuated cell sorting (SAWACS)," Lab Chip **10**(6), 789–794 (2010).
19. G. Destgeer, B. H. Ha, J. H. Jung, and H. J. Sung, "Submicron separation of microspheres via travelling surface acoustic waves," Lab Chip **14**(24), 4665–4672 (2014).
20. C. M. Earhart, C. E. Hughes, R. S. Gaster, C. C. Ooi, R. J. Wilson, L. Y. Zhou, E. W. Humke, L. Xu, D. J. Wong, S. B. Willingham, E. J. Schwartz, I. L. Weissman, S. S. Jeffrey, J. W. Neal, R. Rohatgi, H. A. Wakelee, and S. X. Wang, "Isolation and mutational analysis of circulating tumor cells from lung cancer patients with magnetic sifters and biochips," Lab Chip **14**(1), 78–88 (2014).
21. J. S. Park, S. H. Song, and H. I. Jung, "Continuous focusing of microparticles using inertial lift force and vorticity via multi-orifice microfluidic channels," Lab Chip **9**(7), 939–948 (2009).
22. Z. Wu, Y. Chen, M. Wang, and A. J. Chung, "Continuous inertial microparticle and blood cell separation in straight channels with local microstructures," Lab Chip **16**(3), 532–542 (2016).
23. Y. Chen, P. Li, P.-H. Huang, Y. Xie, J. D. Mai, L. Wang, N.-T. Nguyen, and T. J. Huang, "Rare cell isolation and analysis in microfluidics," Lab Chip **14**(4), 626–645 (2014).
24. Y. Tang, J. Shi, S. Li, L. Wang, Y. E. Cayre, and Y. Chen, "Microfluidic device with integrated microfilter of conical-shaped holes for high efficiency and high purity capture of circulating tumor cells," Sci. Rep. **4**(1), 6052 (2015).
25. C. C. Wong, Y. Liu, K. Y. Wang, and A. R. A. Rahman, "Size based sorting and patterning of microbeads by evaporation driven flow in a 3D micro-traps array," Lab Chip **13**(18), 3663–3667 (2013).
26. X. Li, W. Chen, G. Liu, W. Lu, and J. Fu, "Continuous-flow microfluidic blood cell sorting for unprocessed whole blood using surface-micromachined microfiltration membranes," Lab Chip **14**(14), 2565–2575 (2014).
27. W. Beattie, X. Qin, L. Wang, and H. Ma, "Clog-free cell filtration using resettable cell traps," Lab Chip **14**(15), 2657–2665 (2014).
28. S. M. McFaul, B. K. Lin, and H. Ma, "Cell separation based on size and deformability using microfluidic funnel ratchets," Lab Chip **12**(13), 2369–2376 (2012).
29. J. D. Adams and H. T. Soh, "Tunable acoustophoretic band-pass particle sorter," Appl. Phys. Lett. **97**(6), 064103 (2010).
30. V. Skowronek, R. W. Rambach, and T. Franke, "Surface acoustic wave controlled integrated band-pass filter," Microfluid. Nanofluidics **19**(2), 335–341 (2015).
31. L. Ren, Y. Chen, P. Li, Z. Mao, P.-H. Huang, J. Rufo, F. Guo, L. Wang, J. P. McCoy, S. J. Levine, and T. J. Huang, "A high-throughput acoustic cell sorter," Lab Chip **15**(19), 3870–3879 (2015).
32. Z. T. F. Yu, K. M. Aw Yong, and J. Fu, "Microfluidic blood cell sorting: now and beyond," Small **10**(9), 1687–1703 (2014).
33. J. Xu, D. Wu, J. Y. Ip, K. Midorikawa, and K. Sugioka, "Vertical sidewall electrodes monolithically integrated into 3D glass microfluidic chips using water-assisted femtosecond-laser fabrication for in situ control of electrotaxis," RSC Advances **5**(31), 24072–24080 (2015).
34. S. D. Gittard, A. Nguyen, K. Obata, A. Koroleva, R. J. Narayan, and B. N. Chichkov, "Fabrication of microscale medical devices by two-photon polymerization with multiple foci via a spatial light modulator," Biomed. Opt. Express **2**(11), 3167–3178 (2011).
35. Y. L. Hu, Y. H. Chen, J. Q. Ma, J. W. Li, W. H. Huang, and J. R. Chu, "High-efficiency fabrication of aspheric microlens arrays by holographic femtosecond laser-induced photopolymerization," Appl. Phys. Lett. **103**(14), 141112 (2013).
36. B. Xu, W. Q. Du, J. W. Li, Y. L. Hu, L. Yang, C. C. Zhang, G. Q. Li, Z. X. Lao, J. C. Ni, J. R. Chu, D. Wu, S. L. Liu, and K. Sugioka, "High efficiency integration of three-dimensional functional microdevices inside a microfluidic chip by using femtosecond laser multifoci parallel microfabrication," Sci. Rep. **6**(1), 19989 (2016).
37. C. Zhang, Y. Hu, J. Li, G. Li, J. Chu, and W. Huang, "A rapid two-photon fabrication of tube array using an annular Fresnel lens," Opt. Express **22**(4), 3983–3990 (2014).
38. D. Wu, S. Z. Wu, L. G. Niu, Q. D. Chen, R. Wang, J. F. Song, H. H. Fang, and H. B. Sun, "High numerical aperture microlens arrays of close packing," Appl. Phys. Lett. **97**(3), 031109 (2010).
39. L. Yang, A. El-Tamer, U. Hinze, J. W. Li, Y. L. Hu, W. H. Huang, J. R. Chu, and B. N. Chichkov, "Two-photon polymerization of cylinder microstructures by femtosecond Bessel beams," Appl. Phys. Lett. **105**(4), 041110 (2014).

40. J. Wang, Y. He, H. Xia, L. G. Niu, R. Zhang, Q. D. Chen, Y. L. Zhang, Y. F. Li, S. J. Zeng, J. H. Qin, B. C. Lin, and H. B. Sun, "Embellishment of microfluidic devices via femtosecond laser micronanofabrication for chip functionalization," Lab Chip **10**(15), 1993–1996 (2010).
41. L. Amato, Y. Gu, N. Bellini, S. M. Eaton, G. Cerullo, and R. Osellame, "Integrated three-dimensional filter separates nanoscale from microscale elements in a microfluidic chip," Lab Chip **12**(6), 1135–1142 (2012).
42. D. Wu, S. Z. Wu, J. Xu, L. G. Niu, K. Midorikawa, and K. Sugioka, "Hybrid femtosecond laser microfabrication to achieve true 3D glass/polymer composite biochips with multiscale features and high performance: the concept of ship-in-a-bottle biochip," Laser Photonics Rev. **8**(3), 458–467 (2014).
43. D. Wu, L. G. Niu, S. Z. Wu, J. Xu, K. Midorikawa, and K. Sugioka, "Ship-in-a-bottle femtosecond laser integration of optofluidic microlens arrays with center-pass units enabling coupling-free parallel cell counting with a 100% success rate," Lab Chip **15**(6), 1515–1523 (2015).
44. D. Wu, J. Xu, L. G. Niu, S. Z. Wu, K. Midorikawa, and K. Sugioka, "In-channel integration of designable microoptical devices using flat scaffold-supported femtosecond-laser microfabrication for coupling-free optofluidic cell counting," Light Sci. Appl. **4**(1), e228 (2015).
45. B. B. Xu, Y. L. Zhang, H. Xia, W. F. Dong, H. Ding, and H.-B. Sun, "Fabrication and multifunction integration of microfluidic chips by femtosecond laser direct writing," Lab Chip **13**(9), 1677–1690 (2013).
46. H. Wei, B. H. Chueh, H. Wu, E. W. Hall, C. W. Li, R. Schirhagl, J. M. Lin, and R. N. Zare, "Particle sorting using a porous membrane in a microfluidic device," Lab Chip **11**(2), 238–245 (2011).
47. J. S. Kuo, Y. Zhao, P. G. Schiro, L. Ng, D. S. W. Lim, J. P. Shelby, and D. T. Chiu, "Deformability considerations in filtration of biological cells," Lab Chip **10**(7), 837–842 (2010).
48. Z. Lao, Y. Hu, C. Zhang, L. Yang, J. Li, J. Chu, and D. Wu, "Capillary force driven self-assembly of anisotropic hierarchical structures prepared by femtosecond laser 3D printing and their applications in crystallizing microparticles," ACS Nano **9**(12), 12060–12069 (2015).
49. Y. Hu, Z. Lao, B. P. Cumming, D. Wu, J. Li, H. Liang, J. Chu, W. Huang, and M. Gu, "Laser printing hierarchical structures with the aid of controlled capillary-driven self-assembly," Proc. Natl. Acad. Sci. U.S.A. **112**(22), 6876–6881 (2015).
50. Z. Zhang, J. Xu, B. Hong, and X. Chen, "The effects of 3D channel geometry on CTC passing pressure--towards deformability-based cancer cell separation," Lab Chip **14**(14), 2576–2584 (2014).
51. Z. F. Zhang, X. L. Chen, and J. Xu, "Deformability-based circulating tumor cell separation with conical-shaped microfilters: Concept, optimization, and design criteria," Biomicrofluidics **9**, 024108 (2015).
52. H. Mohamed, M. Murray, J. N. Turner, and M. Caggana, "Isolation of tumor cells using size and deformation," J. Chromatogr. A **1216**(47), 8289–8295 (2009).
53. W. Liu, J. C. Wang, and J. Wang, "Controllable organization and high throughput production of recoverable 3D tumors using pneumatic microfluidics," Lab Chip **15**(4), 1195–1204 (2015).
54. X. Wang and I. Papautsky, "Size-based microfluidic multimodal microparticle sorter," Lab Chip **15**(5), 1350–1359 (2015).
55. H. Kim, S. Lee, J. H. Lee, and J. Kim, "Integration of a microfluidic chip with a size-based cell bandpass filter for reliable isolation of single cells," Lab Chip **15**(21), 4128–4132 (2015).

1. Introduction

Microfluidic chips technology has received significant attentions because of their distinct advantages such as low reagent consumption, high integration level, high processing speed, good portability and miniaturization [1–3]. It has been recognized as one of the world-changing technologies and to date, has been applied in diverse fields ranging from chemistry, biology, materials, to environmental science and tissue engineering [4–7]. Specially, cell sorting [8–12] is of great importance to enrich or purify biosamples into well-defined populations for a variety of applications, such as single cell sequencing and drug screening.

A variety of microfluidic sorting methods [13,14] have been developed to separate microparticles based on either size, shape, density, deformation, electrical polarizability, magnetic susceptibility or surface chemical properties. Both of the external-force-based and non-external-force-based approaches have been demonstrated. External-force-based approaches employ external sources such as optical tweezers [15,16], standing surface acoustic wave [17–19] or magnetic forces [20], most of which are expensive, complicated and inconvenient, making them difficult to be integrated with functional lab-on-a-chip components. Compared to external-force-based approaches, non-external-force-based microfluidic techniques such as hydrodynamic filtration [21,22], pinched flow fractionation [23] and micropore membranes [24–26] simplify the design, fabrication procedure and operation of devices. Among those techniques, micropore membranes offer one of the simplest sorting scheme and can be easily operated without external actuation. However, the micropore membranes suffer from two major issues. The first is clogging [27,28] caused by

microparticles trapping and aggregation formation around micropores. It prevents subsequent particles from passing through the pores and alters the hydrodynamic resistance of the membrane in an unpredictable way. The second is that most of the micropore membranes have a limited capability that only the particles smaller than a specific size can be filtered [29,30]. In other words, they can only capture large microparticles and release small ones. Capturing small particles and releasing large particles or capturing median size particles and releasing other size particles cannot be achieved by the conventional micropore membranes. In practical biological researches, the cells always have polydisperse distributions and cells with a specific size range need to be sorted out from a bulk cells suspension [31,32]. All of the above issues further enhanced the demands for new design of high performance microsorters.

To overcome these issues, we propose a novel architecture which can perform multimodal (low-, band- and high-capture) and clogging-improved sorting. The designed microsorter has a unique arch-like shape which is composed of a couple of microgrid filters with different filtering sizes. The filtering sizes of front and back filter are designed to be larger and smaller than the size of target particles, respectively. As a result, the target particles can pass through the front filter, while be trapped by the back filter. Additionally, the larger particles pass over the top of the sorter, and the smaller ones pass through both the front and back filter. To improve clogging throughout the sorting process, the designed sorter has a height lower than that of the microchannel. Using femtosecond laser parallel multifocal fabrication, the arch-like microstructures are successfully integrated inside a 'Y'-shaped microchannel with faster fabrication speed than the conventional single femtosecond laser polymerization. By using this novel sorters design, particles with 2.5 μm, 5 μm or 10 μm were successfully sorted. The clogging-improved performance of the sorters was also investigated. At last, preliminary validation of the device in SUM159 breast cancer cells separation from blood cells was demonstrated. The separation efficiency and the purity is about 78% and 88% respectively. Our approach offers a number of benefits, including fast microsorter fabrication, precise and controllable filtering size design, high separation resolution, clogging-improved and easy operation.

2. Methods

2.1 Fabrication of a 'Y'-shaped glass microchannel

A Foturan glass (Schott Glass Corp) was irradiated with femtosecond laser using an objective lens (NA 0.46). The sample was then annealed in a furnace to form a crystalline phase of lithium metasilicate. The annealed microchip was followed by chemical etching in an ultrasonic bath with a 10% hydrofluoric acid (HF) solution to selectively remove the crystalline phase. At last, the sample was treated with a second annealing to improve the surface quality. More details of fabrication procedure is available elsewhere [33]. The 'Y'-shaped channel with a width of about 110 μm and a depth of 60 μm was used.

2.2 Femtosecond laser multifocal integration of the arch-like microsorter

The 3D microstructure was fabricated by femtosecond laser (800 nm) two-photon polymerization because of its distinct advantages, such as the programmable designability, 3D processing capability and high spatial resolution. The glass microchip was firstly coated with a hybrid organic-inorganic sol-gel SZ2080 (IESL-FORTH, Greece) and prebaked at 100 °C for 90 minutes. A phase-modulated reflective liquid-crystal spatial light modulator (Holoeye, Pluto NIR-2) was applied to display the computer generated hologram (CGH). Then the phase-modulated laser beam was focused by a $60 \times$ objective lens (oil-immersed, NA 1.35). In order to reduce the processing time, parallel multifocal (5 foci) processing method was applied by a pre-designed CGH [Fig. 1(a)]. The periodic microsorter was divided into 5 parts and each part was solidified by a focal spot layer-by-layer scanning. To ensure the

sorter adhering the channel tightly, the sorter was designed to be a bit wider than that of the channel. The structures polymerized by each focus scanning overlapped each other to further enhance its robustness. After polymerization, the sample was developed in 1-propanol for 30 minutes. Finally, a PDMS (Dow Corning, United States) slab was covered on the glass surface to form a closed microfluidic chip. The fabrication time is about 30 minutes in our experiments.

2.3 CGHs generation

The 5 spot pattern was firstly designed, and the desired CGH was generated by using a weighted Gerchberg-Saxton (GS) algorithm [34–36]. The intensity of each spot in desired multifoci pattern was monitored during iteration, and corresponding weighting factors were employed to update the original target field pattern in the next iterative loop to get better uniformity. The CGH with 1080×1080 pixels was displayed in the center region of the SLM, which had 256 gray levels corresponding to phase modulation from 0 to 2π. The power utilization efficiency of 5 foci was about 36%.

2.4 Microparticles sample preparation

Silicon dioxide ($SiO2$) microspheres (Huge Biotech Corp, China) with diameters of 10.0, 5.0 and 2.5 μm were mixed in alcohol solution. The concentration of the bead suspensions was 10^4 ml^{-1} in our experiments and the flow speed was about 100-400 μm/s. The SUM159 triple-negative breast cancer cell line was grown in 60 mm petri dishes using the recommended culture conditions as described previously [36]. Cells were treated with Trypsin-EDTA (Gibco, United States) solution after they became confluent for 1 minute. Cell suspensions were then centrifuged at 1000 rounds per minute for 5 minutes in a centrifuge tube. New culture media were added after removing the supernatant and cells were resuspended by gently pipetting several times. The cells were labeled with red fluorescent protein (Dsred) to observe the sorting process more visibly. Prior to sorting tests, human blood was collected from healthy donors in a collection tube with EDTA to prevent coagulation. The human blood was firstly diluted 10^4 times in PBS, then about 100 breast cancer cells were added into the diluted blood sample.

3. Results and discussion

3.1 Multifocal parallel microstructures integration inside a 'Y'- shape channel

In recent years, femtosecond laser [37–39] multifocal parallel microfabrication [36] has been recognized as a powerful tool to integrate 3D microstructures inside a microfluidic chip [40–45] due to higher processing speed with the same precision compared with the conventional single femtosecond laser scanning. Figure 1b shows a schematic illustration of laser fabrication system, in which CGH [Fig. 1(a)] is displayed on a SLM [Fig. 1(b)] for shaping the laser beam into multifoci beam [Fig. 1(c)]. Based on the width of the microchannel and the sorter design, we design a CGH [Fig. 1(a)] to generate 5 foci [Fig. 1(c)]. In order to achieve multi-mode microparticles sorting, here, a novel arch-shape microsorter design is demonstrated. The detail of the new design is described in next section. Image of the microchannel is showed in Fig. 1(e).
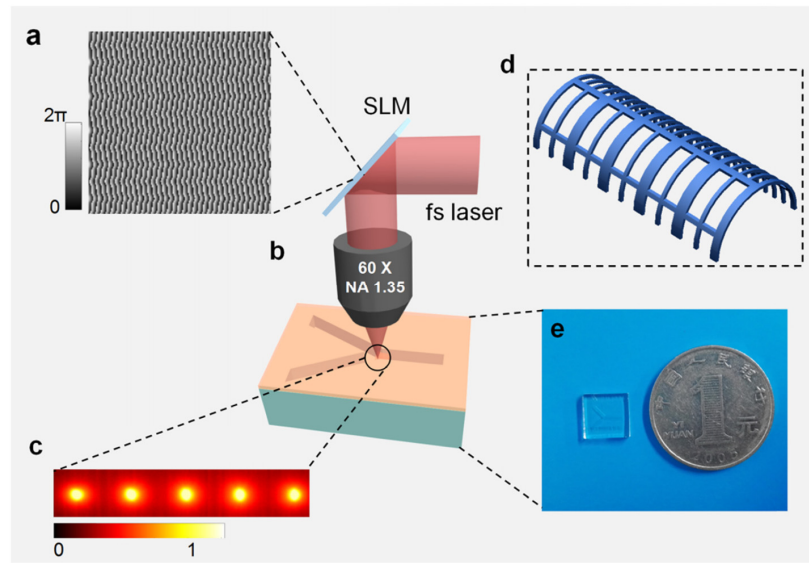
Fig. 1. Femtosecond laser multifocal integration of 3D arch-like sorter inside a 'Y'-shaped microchannel. (a) shows the CGH displayed on the SLM for generating the 5 foci. (b) Schematic illustration of system for femtosecond laser multifocal parallel integration of microsorters. (c) The generated 5 foci intensity distribution. (d) A novel arch-shape microsorter design. (e) Photograph of the 'Y'-shaped microchannel in comparison with a one China Yuan coin.

3.2 Novel arch-like structures design

Conventional micropore membranes [24–26,46] are typically formed into a pre-prepared microfluidic microchannel perpendicular to the sample flow direction to construct a sorter or filter. Most membranes have a plenty of round micropores [46] with a single filtration diameter or microgrids [47] with a fixed width (Fig. 1a). One issue of these membranes is clogging. Specifically, the bigger microparticles block the micropores, which leads to any microparticles impossible to pass through the micropores. Then the microparticles adhere to the sorter or the channel walls, finally leading to the complete clogging of the sorter. Crossflow filter reduced the incidence of clogging instead of having a filter normal to the flow. However, the clogging was still unresolved and general crossflow devices limited the practical use due to the inability to precisely control the force used to deform cells across the membrane. Compared with the micropores, microgrids can reduce the clogging, even if a microgrid aperture traps multiple microparticles simultaneously, interstitial spaces between close-packed microparticles are still likely available for fluid flow [47]. Moreover, the grid can reduce the cell damage caused by unrecoverable deformation of cells [47], because the pressure differences of passing cells through the microgrid is distinctly different from that of the micropores [Fig. 2(a) and 2(b)]. For example, when the flow speed is 1.5 m/s, the pressure differences of 655 Pa for the microgrids filter is much smaller than about 1210 Pa for the micropores filter. The larger pressure difference can lead to the cell deformation excessively and increase the possibility of the cell damage. Although the microgrid membrane has a better performance, the clogging is still a serious issue remaining unresolved [Fig. 3(a)].
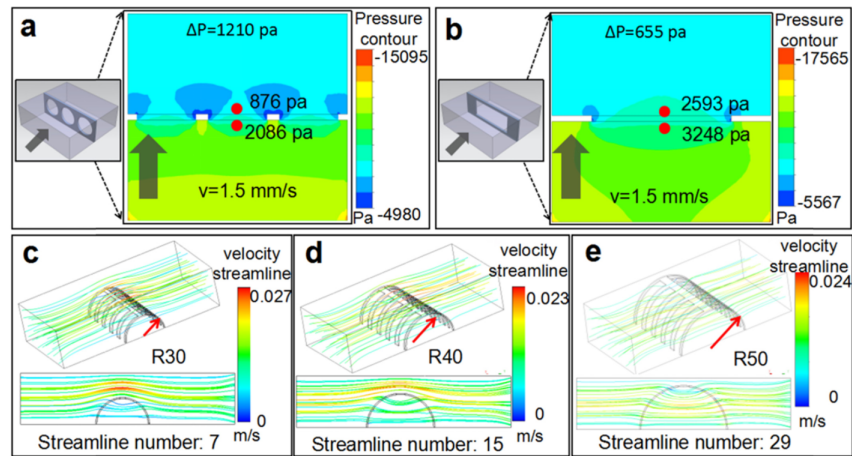
Fig. 2. Fluid simulations of conventional micropore and microgrid sorters and the novel arch-like microsorter. a and b are the fluid simulation results of the pressure difference when liquid flows are 1.5 mm/s speed, respectively. The two filters have the same filtering area. The pressure difference of the micropore filter is much larger than that of the microgrid filter, which may induce the cell deformation excessively resulting in cell damage. c, d and e show the fluid simulation results of the arch-like microsorters with different height design (30, 40 and 50 μm) to optimize the design. More flow line passing through the microsorter means that much more particles will be captured by the arch-like sorter.

Another issue of the micropore and microgrid menbranes is that these menbranes only allow to separate microparticles whose size is larger than a specific size (high-capture filters) and are incapable of purifying target species with a specific range of sizes, e.g., band-capture filters. Specifically, when a filter with a filtering size of 10 μm is designed to separate a mixed sample (5-20 μm), only particles (10-20 μm) larger than the filtering size can be separated. Sorting particles with a particular range of sizes (e.g., 7-15 μm, or 12-17 μm) cannot be achieved in spite of the fact that the any size-ranging sorting is highly requested for many applications.

Figure 3(b) shows our new concept design of sorters with an arch-like architecture inspired by the Chinese arch-bridges which can improve their robustness. Unlike the conventional one, the new sorter is composed of two filters with different filtering sizes and its height is designed to be 40 μm lower than the microchannel height (60 μm). The sorter has an arch-bridge-like shape with a semi-circle cross-section. The lower height design is essential for clogging-improved and long-time operation. Figure. 2(c), (d) and (e) show the simulated results of fluid flow for the sorters with different heights. The higher height will lead to much more streamlines pass through the sorter and increase the possibility of particles capture. Although the sorter with 50 μm height has the highest possibility of particles capture than the ones with 40 and 30 μm height, the sorter with 40 μm height was chosen in actual usage because the sealing of microchip with PDMS may decrease the final microchip height (<50 μm) due to pressure. Figure 3(b) shows the schematic diagram of size-selective separation of the target microparticles (the median) from a mixed particles sample with three different sizes. Here, the front filtering size is designed to be larger than the size of target median particles but smaller than the largest particles, while the back filtering size is smaller than the target particles but larger than the smallest ones. The streamlines are shown in the right of Fig. 3(b), exhibiting that the particles larger than the front filtering size bypass the 3D sorter, while the smallest particles are captured inside the sorter. Figure 3(c) left is a high-capture sorter which enables to capture the largest particles from three different size particles. In this case, the front filtering size is larger than the biggest particles and the back one is smaller than the biggest particles but larger than the other two particles. Figures 3(c) middle

and right show a band-capture and low-capture sorters for sorting the interested median and smallest size microparticles. The particle size distribution before and after sorting are sketched in Fig. 3(c). The flexible sorting of any size-ranging particles will be possible by designing appropriate filtering sizes of the front and back filters based on the above concept.
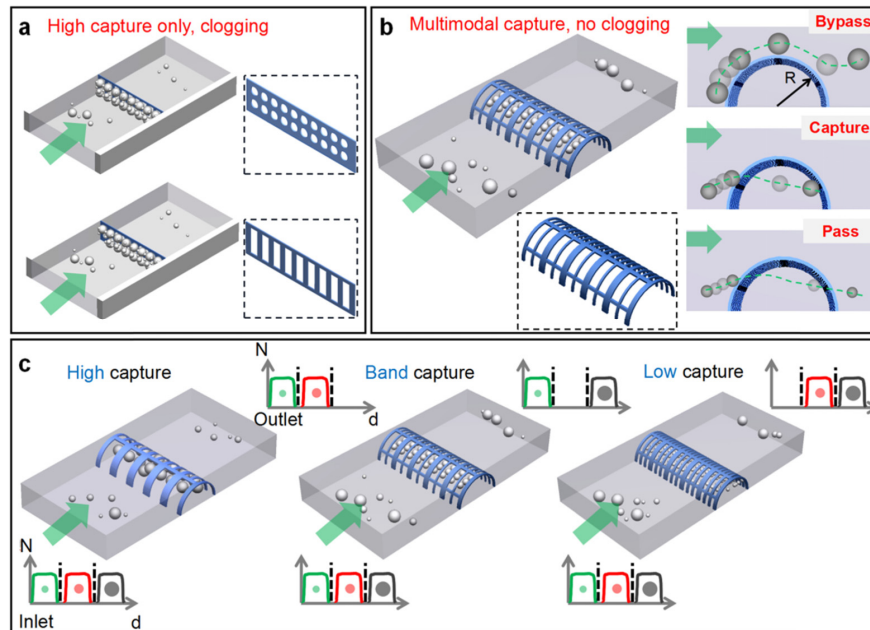

Fig. 3. Schematic illustration of the novel multimodal and clogging-improved sorters. (a) The conventional micropore (upper) and microgrid (lower) filtering membranes. They can only separate particles with a single specific size and have an issue of clogging. (b) The new arch-like design. The image shows the band-capture sorting mode that the larger particles bypass the sorter, theand smaller pass through the sorter, while the median particles are captured by the arch-like structure. (c) shows the high-capture, band-capture and low-capture sorting modes (left to right). The high-capture sorting mode targets to capture the largest particles. The inset schematics indicate particle size distribution before and after sorting. d and N represent particle size and number, respectively. The target particles of band-capture and low-capture sorting mode are the median and smallest particles, respectively.

3.3 Fast microsorters integration

Schematic diagrams of three different sorters (low-capture, band-capture and high-capture) fabricated by femtosecond laser 5 foci are shown in left column of Figs. 4(a), 4(b) and 4(c). All sorters have a periodic structure with 40 μm height (right column of Figs. 4(a), 4(b) and 4(c)). SEM and CCD images [Fig. 4(h) and 4(i)] show that the microstructures are standing steadily in the microchannel. Some deformations formed in the grids [Fig. 4(d)] are caused by capillary force during the liquid evaporation [48,49]. By pumping the liquid sample into the channel, the deformations disappear and the sorter recovers to its original design [Fig. 4(e)] which will not influence the sorting function due to the reversibility of capillary force.
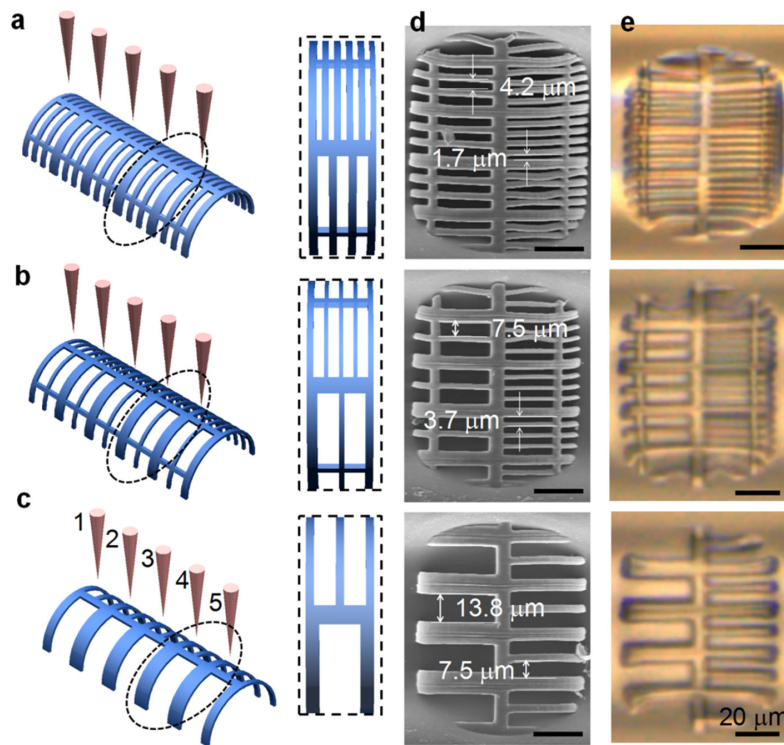
Fig. 4. Femtosecond laser multifocal integration of 3D arch-like sorter inside a 'Y'-shaped microchannel. (a) (b) and (c) show multi-focal fabrication of arch-like 3D microsorter of low-capture (2.5 μm), band-capture (5 μm) and high-capture (10 μm) sorters, respectively. In view of the width of microchannel and periodic sorter design, 5 foci are chosen for faster integration. The right column shows periods of each sorter. (h) SEM images of the three sorters for 2.5 μm, 5 μm and 10 μm particles sorting, respectively. (i) shows the sorters immersed in water.

3.4 Multimodal sorting of microparticles

In order to test the function of the sorter, 2.5, 5, and 10 μm-diameter silicon dioxide (SiO2) micro-spheres were introduced into the inlet. Figure 5(a) shows the time-lapsed optical microscopy images of the low-capture sorting mode. It can be clearly identified [Fig. 5(a), See Visualization 1] that both the 10 and 5 μm particles (larger than the front filtering size (4.2 μm)) bypass the low capture sorter, while 2.5 μm particles (smaller than the front filtering size (4.2 μm) and larger than the back filtering size (1.7 μm)) are trapped inside the sorter [Fig. 5(a)]. This result proves that our design is effective for low-capture sorting. Figure 5(b) shows the particle size distributions for the low-capture sorter in the inlet, sorter and outlet. The sorter only contains the smallest size particles (2.5 μm) demonstrating that the purity of the low capture sorter is 100%. Here, the purity is defined as the percentage of the target particles among all the particles inside the sorter. The band- and high-capture sorters also can successfully achieve their targeted particles (5 and 10 μm) sorting. Time-lapsed optical microscopy images of the band and high capture mode sorting are shown in Fig. 6. For these two sorting modes (See Visualization 2 and Visualization 3), the majority of particles captured inside the microsorters are the target particles with the purity of 92% (band-capture) and 86% (high-capture) [Figs. 6(c) and 6(d)]. The novel microsorter is distinct from a standard filter membrane which only shows the ability to capture large particles and release small ones. Note that most of the targeted microparticles are captured inside the arch-like

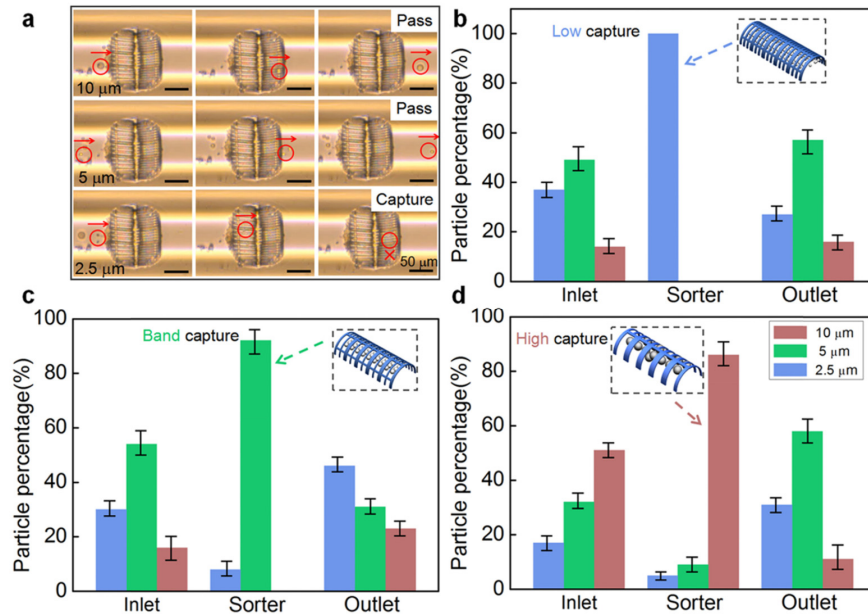microsoters while a small portion of them can also flow along the streamline to bypass the sorter.

Fig. 5. Multimodal sorting microparticle mixtures into different size ranges. (a) shows time-lapsed optical microscopy images of the low-capture sorting mode. 10 and 5 μm silicon dioxide micro-spheres bypass the sorter, while a 2.5 μm microsphere is captured by the sorter. (b) The percentage of each particle by low-capture sorting mode. SE is evaluated to be 100%, which means that the sorter contains only 2.5 μm microspheres. (c) and (d) show the percentage of each particle by band-capture and high-capture sorting mode, respectively. SEs are about 92% for band-capture sorter, and 86% for high-capture sorter. There are no 10 μm particles in the band-capture sorter. The high-capture sorter contains few 2.5 and 5 μm microspheres.

The extraction of separated particles is very critical for downstream molecular analysis and other studies. In our device, firstly the particles suspension is introduced into the lower inlet of the 'Y'-shape microchannel [Fig. 7], valve 1 (the other inlet) is closed and particles are directed through the main flow channel. Several minutes later, the arch-like microsorter is full of targeted particles (e.g. 10 μm microparticles). Then valve 2 is closed and alcohol solution is injected into the outlet in order to flush the 10 μm microparticles to valve 1 to collect them. As a proof-of-concept demonstration, our extraction method is convenient and takes full advantage of the 'Y'-shape microchannel. We can also integrate high- and band-capture sorters inside a microchannel for simultaneously sorting 10 and 5 μm microparticls [Fig. 6(g)]. By arranging different sorters in series in the channel, particles with different range of sizes (e.g., 7-10 μm and 13-16 μm particles from a mixed sample (5-20 μm)) can be separated simultaneously.
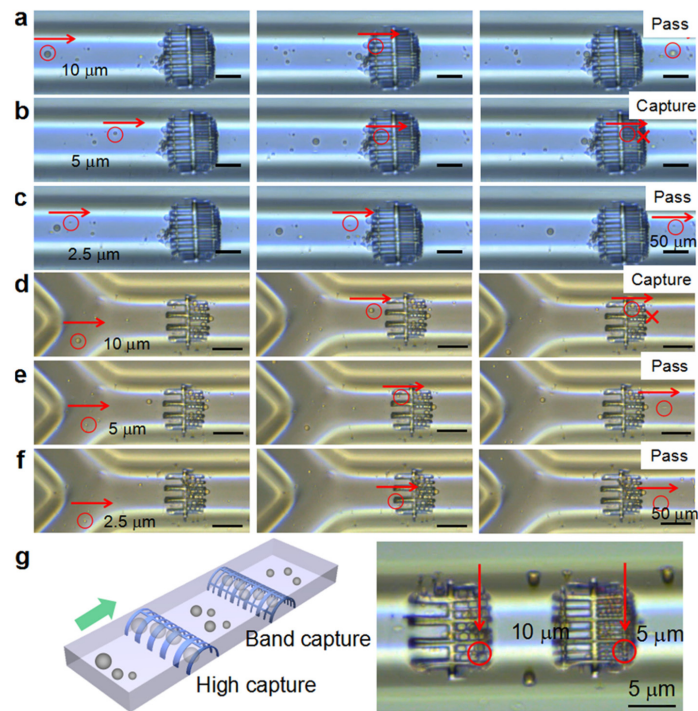
Fig. 6. Multimodal microsorters integrated for multi-size-range sorting. (a) (c) and (b) show time-lapsed optical microscopy images of a 10 and 2.5 µmmicroparticles bypassing the band-capture sorter and the capture process of the target particles (5 µm). (d) (e) and (f) displays the capture process of the target particles (10 µm) and 5 and 2.5 µm microparticles bypassing the sorter. (g) shows the schematic diagram of the multi-size-range sorters. The largest particles are captures by the high-capture sorter first, while the median particles are sorted by the band-capture sorter arranged after the high-capture sorter.The smallest particles are exhausted to the outlet.
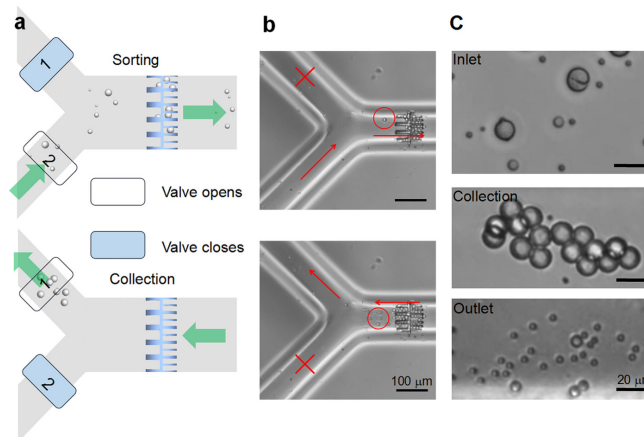

Fig. 7. Procedure for sorting and collecting particles. In the sorting process, firstly the particles suspension is introduced into the one inlet (lower inlet) of the Y-shape microchannel. Particles are directed though the mainflow channel. Several minutes later, the arch-like microsorter is full of targeted particles. Then valve 2 is closed and alcohol solution is injected into the outlet in order to flush the 10 µm Sio2 microparticles to the one side of inlet (valve 1). (b) shows time-lapsed optical microscopy images of the target particles collection process. (c) are the optical microscopy images of particles introduced into the inlet, the collected targeted-particles and the particles in the outlet, respectively.

3.5 Clogging-improved performances of the arch-like sorters

Micropore and microgrid membranes limit their applications [27,28] because of the clogging issue. Crossflow microfluidic devices [24] can lessen the clogging effectively by adding a perpendicular component to the devices to prevent the membrane from being directly impacted by the fluid. However, general crossflow devices have a drawback that cannot precisely control the force used to deform cells across the membrane. Microfluidic funnel ratchets and oscillatory flow [28] can reduce the clogging by periodically removing particles that accumulate in the filter. The operation process is relatively complex and time-consuming. Resettable microdevices [27] based on the concept of external pressure control can prevent clogging and adsorption by periodically clearing the filtration microstructures to allow sustainable operation. The device size is often large, and a complex operation is required. The sorter with a well-designed height and an arch-like architecture not only ensures the high capturing efficiency (CE) which is defined as the percentage of the target particles inside the sorter among all the target particles introduced in the inlet, but also achieves long time clogging-improved operation. The new design of the sorter proposed here can avoid clogging for as long as 25 minutes. A conventional membrane filter only permits capturing large microparticles while release small microparticles. After a vast variety of large particles stopped and accumulated, the standard membrane filter will be clogged and lose its separation ability. It need to be highlighted that the particles aggregation directly leads to clogging which prevents the subsequent particles from passing through the filters and alters the hydrodynamic resistance of the membrane in an unpredictable way. The new arch-like microstructures is not prone to be blocked and not easy to form particles aggregation because there is enough space for the microparticles to pass over. Several minutes later, the arch-like microstructures is full of targeted microparticles, then the following microparticles will bypass the microstructure. Figure 8 shows the clogging-improved performances of the three sorters. After 20 minutes, the low-capture sorter is still free of clogging and the liquid can still flow through the sorter [Fig. 8(a)]. The CE of high-, band- and low-capture sorter is ~86%, ~54% and ~31%, respectively. We believe that 40 μm height of sorters designed can give the best balance between the clogging-improved property and high CE. CE will be further improved by using a deeper channel or operating at a lower flow speed. The band- and high capture sorters [Figures. 8(b) and 8(c)] also show clogging-improved property similar to the low capture sorter. After 10 min. and 6 min., the band capture and the high capture sorters are still free of clogging and the liquid can still flow through the sorter.

Here, the maximum processing volume of samples is about 100 μl with sample concentration of 10^4 ml^{-1} in this device. Before the device clogs, about 1000 beads could be processed. Compared with the usage of a straight channel, the 'Y'-shaped channel can help one to extract the targeted particles to the other inlet of the Y-shaped channel when the microsorters are clogged and then continue to process the samples from the inlet. In this way, the microsorters are more clogging-improved as more volume of samples could be processed on the same chip. The microchip can be cleaned by injecting the deionized water into the outlet. After a few seconds, all spheres have been cleared out of the sorter and then the chip can be reused for several times.
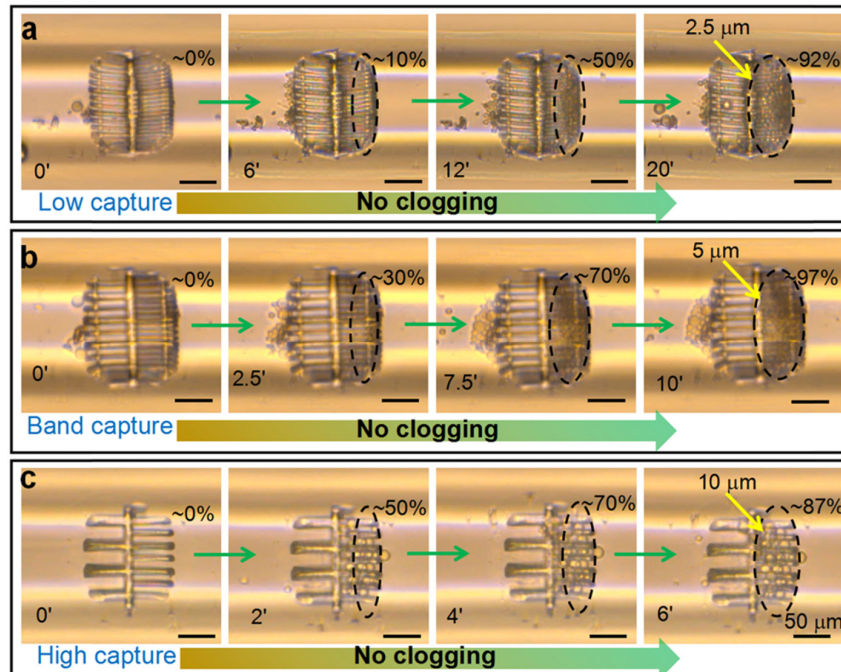
Fig. 8. Clogging-improved property of the arch-like microsorters. (a) shows the time-lapsed microscope images of the low-capture sorter. After about 20 minutes, the sorter is filled with 2.5 μm particles, while no-clogging happens. (b) Time-lapsed microscope images of the band-capture sorter. 10 minuters later, about 97% in space of the sorter is occupied with 5 μm particles. (c) shows the flowing process of 10 μm particles.

3.6 Sorting of cancer cells from human blood

The sorting of cancer cells in peripheral blood of cancer patients are intrinsically important because cancer cells in peripheral blood are reliable biomarkers for metastatic detection and treatment monitoring [24]. Here, we demonstrate that the sorter successfully separates SUM 159 triple-negative breast cancer cells (sizes ranges from 10 to 20 μm) [36] from human blood. The disc-shape red blood cells (diameter of 6-9 μm and thickness of about 2 μm) with highly deformability and platelets with a size of 2-3 μm can pass freely through the microsorters (the front filtering size is 17 μm and the back one is 10 μm), while the white blood cells (10-18 μm) with their size distribution overlapping with that of cancer cells (10-20 μm) influence the separation performance of the microsorters and design should take into consideration for this issue. Both cancer cells and normal white blood cells vary significantly in size and deformability. One consistent finding has been observed, that is, cancer cells are typically larger and stiffer than normal blood cells for solid tumors [50]. Note that a more deformable cell possesses a lower interfacial tension coefficient (ITC) [51]. The interfacial tension coefficient of white blood cells is 0.027 mN/m which is lower than that of the breast cancer cells (with an ITC>7 mN/m). It means that the white blood cells are easier to deform to pass through the microsorters than the breast cancer cells. Effective cancer cells capturing has been reported with a filtering size in the range of 5-12 μm [52]. The smaller filtering size the microsorter has, the larger possibility the white blood cells being captured. When the back filtering size is 5 μm, many white blood cells are captured inside the arch-like microsorters, which lowers the purity of the captured cancer cells. If the back filtering size is 12 μm, there are fewer or no white blood cells captured while several small cancer cells passed through the microsorters, which lowers the capture efficiency of cancer cells. In order to reach a good balance between capture efficiency and purity of cancer cells, the median size of the backing

filtering size (10 μm) was chosen. Figure 9(a) shows an optical microscope image of the blood sample before sorting. For better observation, fluorescence microscope is employed to characterize the cancer cells [Fig. 9(a) right] which are labeled with red fluorescent protein (Dsred). Figures 9(c), 9(d) and 9(e) clearly show that blood cells pass through the sorter (see Visualization 4) while cancer cells (see Visualization 5 and Visualization 6) are captured inside the sorter. We need to point out that the particles moving at different heights are caused by the steamline and this phenomenon is reasonable. The trapped cancer cell can further influence the streamline distributions, that is why some particles moving around the sides of the filters. The capture efficiency and recovery rate of cancer cells were about 88% and 78%. After sorting, the sorter is filled with cancer cells [Fig. 9(b)], which can be used for subsequent inspection and investigation [53].
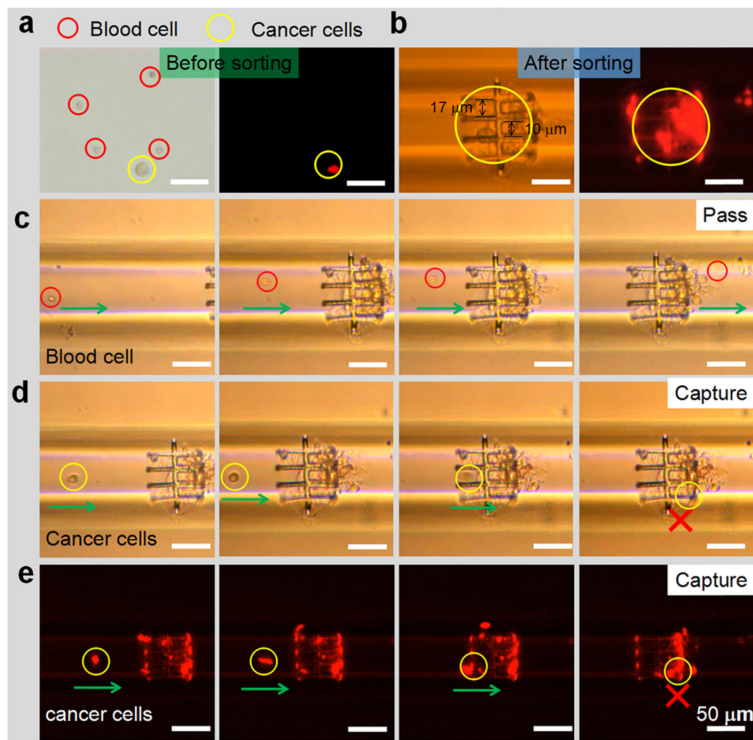

Fig. 9. Demonstration of sorting of cancer cells from human blood. (a) Optical (left) and fluorescence microscope (right) images of the blood sample including cancer cells before sorting. The red circle indicates blood cells and the yellow one indicates cancer cells which are labeled with red fluorescent protein. (b) The sorter is filled with cancer cells after sorting. (c) shows the flowing process of a blood cell (~7.6 μm) passing over the high-capture sorter. (d) and (e) show the time-lapsed microscope images and fluorescence images of a cancer cell (~14 μm) being captured inside the sorter, respectively.

4. Conclusion

We have proposed a novel arch-like microsorter consisting of a couple of microgrid filters. The microsorters offered versatile capabilities of multimodal (high-, band- and low- capture modes) separation. They were fabricated inside a microchannel by femtosecond laser 3D parallel multifocal. Compared with inertial microfluidics sorting methods [54], extreme flow velocities were not required. Also this arch-like sorter does not need external interdigitated transducers which is difficult to be integrated into the existing microdevices, unlike acoustic wave sorting [29,30]. The high performance of this device is also validated by successful enrichment of SUM 159 triple-negative breast from human blood. In addition to the unique

multimodal particles sorting, our approach offers a number of benefits. Firstly, the new design permits the front and back sorting sizes to be flexibly and precisely adjusted. It is expected that particles with size difference less than 1 μm can be separated using this design by taking account of high fabrication resolution of femtosecond laser processing. The fabrication speed is much faster than the conventional femtosecond laser processing as the parallel multifoci method is utilized. Secondly, the device has a single inlet employing only one syringe pump for sample delivery which greatly reduces the complexity of external devices. Thirdly, clogging-improved operation can last for a long time. We envision that this multimodal and clogging-improved sorter may find a wide range of applications in cell washing, CTCs separation, blood cells sorting, microparticle purification [55], cellular sample preparation, biomedical research and 3D tumor generation.